Collective polaritonic effects on chemical dynamics suppressed by disorder

Juan B. Pérez-Sánchez ◉,[1] Federico Mellini ◉,[1] Noel C. Giebink,[2] and Joel Yuen-Zhou ◉[1]

[1]*Department of Chemistry and Biochemistry, University of California San Diego, La Jolla, California 92093, USA*

[2]*Department of Electrical Engineering and Computer Science, and Physics, University of Michigan, Ann Arbor, Michigan 48109, USA*

We present a powerful formalism, disordered collective dynamics using truncated equations (d-CUT-E), to simulate the ultrafast quantum dynamics of molecular polaritons in the collective strong coupling regime, where a disordered ensemble of $N \gg 10^6$ molecules couples to a cavity mode. Notably, we can capture this dynamics with a cavity hosting a single *effective* molecule with $\sim N_{bins}$ electronic states, where $N_{bins} \ll N$ is the number of bins discretizing the disorder distribution. Using d-CUT-E we conclude that strong coupling, as evaluated from linear optical spectra, can be a poor proxy for polariton chemistry. For highly disordered ensembles, total reaction yield upon broadband excitation is identical to that outside of the cavity, while narrowband excitation produces distinct reaction yields solely due to differences in the initial states prepared prior to the reaction.

I. INTRODUCTION

Molecular polaritons are quasiparticles formed when molecules are strongly coupled to photons trapped in an optical cavity. These systems exhibit many exotic phenomena attributed to the hybridization of collective material polarization and optical field resonances, and have garnered significant attention as they hold the potential to modify energy transfer mechanisms and enhance chemical reactivity without the need for catalysts [1–17]. In the most common scenario, strong light-matter coupling is achieved by a macroscopic number of molecules N, where their *collective* interaction with the optical mode exceeds the cavity and molecular linewidths. Theoretical methods that can incorporate effects of intermolecular interactions [18–20], multiple optical cavity modes [21–23], complex vibrational and electronic structure [24–32], and molecular disorder [23,33–42], while considering a large number of molecules, are in much need to explain experimental observations.

Disorder is an unavoidable feature that can impact polariton transport [43–46], vibrational dynamics [34], superradiance [47], and polaron photoconductivity [48]. In this article, we generalize our recently developed collective dynamics using truncated equations (CUT-E) method [49], which allows efficient modeling of the quantum molecular dynamics of an arbitrarily large number of identical molecules, to study disordered ensembles. At the core of CUT-E lies the exploitation of permutational symmetries [19,47,49–54], which scales the

problem from an ensemble of $N \to \infty$ identical molecules down to a single *effective* molecule strongly interacting with the cavity mode. This effective molecule differs from an actual single molecule in that its strong coupling to the cavity occurs *solely* at the Franck-Condon (FC) region. We lift the constraint of identical molecules, coarse-grain the disorder distributions, and apply permutational symmetries among molecules that belong to the same disorder "bin." This approach is numerically exact for sufficiently short propagation times, where the number of disorder bins required to reach convergence (denoted as N_{bins}) is much smaller than N. This seemingly simple strategy has powerful consequences: the resulting d-CUT-E method maps a disordered molecular ensemble into a single effective molecule, with amplified number of electronic degrees of freedom (DoF) by N_{bins}. This is both conceptually insightful and computationally efficient compared to conventional methods that include every molecule of the ensemble explicitly. Although our method is general and can be applied to arbitrary disorder distributions of the parameters that shape the potential energy surfaces (PESs), here we focus on Gaussian exciton-frequency disorder and study its impact on various ultrafast molecular and optical polaritonic properties.

Our study shows that (1) broadband excitation can modify the reaction yield of the ensemble; however, in the large disorder regime, such changes can be explained just by changes in cavity leakage, despite the presence of the polariton bands in the absorption spectrum; and (2) narrowband excitation can modify the reaction yield even in the large disorder regime. In this case, external narrowband laser and strong light-matter coupling allows the selective excitation of high-frequency vibrational states near the upper polariton (UP) band, which are more reactive than the corresponding excitations of the lower polariton (LP) band. Since the polariton processes involved in the preparation of these states vanish before the reaction ensues, this phenomenon should be interpreted as an optical effect and not as a chemical one.

II. METHOD

To illustrate the method, we assume a single-cavity mode, neglect intermolecular interactions, and restrict ourselves to the first excitation manifold. Our molecular model consists of a ground electronic state and two diabatically coupled excited electronic states, where only one of them can couple to the cavity mode. The molecular model is intentionally simplified to uncover the universal photochemical and photophysical behavior of molecular polaritons. In the CUT-E formalism, each disorder bin is represented by a single effective molecule with a collective coupling $g\sqrt{N}\sqrt{P_i}$, with P_i being the fraction of molecules in the i-th bin. Assuming that the molecules are initially in the global ground state, the CUT-E effective Hamiltonian in the large N limit is given by (see Appendix for details)

$$
\begin{aligned}
\hat{H}'_{\text{eff}} &= \omega_c |1\rangle\langle 1| + \sum_i^{N_{\text{bins}}} \left[-\frac{1}{2}\frac{\partial^2}{\partial q_i^2} + V_{e_1,i}(q_i) \right] |e_{1,i}\rangle\langle e_{1,i}| \\
&+ \sum_i^{N_{\text{bins}}} \left[-\frac{1}{2}\frac{\partial^2}{\partial q_i^2} + V_{e_2,i}(q_i) \right] |e_{2,i}\rangle\langle e_{2,i}| \\
&+ g\sqrt{N}\sum_i^{N_{\text{bins}}} \sqrt{P_i}(|e_{1,i}\rangle\langle 1| + |1\rangle\langle e_{1,i}|)\mathbb{P}_i \\
&+ v_{12,i}|e_{1,i}\rangle\langle e_{2,i}| + \text{H.c.}.
\end{aligned}
\tag{1}
$$

Here, q_i is the vector of mass-weighted coordinates of all vibrational degrees of freedom of molecule i; $|g_i\rangle$, $|e_{1,i}\rangle$, and $|e_{2,i}\rangle$ are the ground and excited electronic states; $V_{g/e_1/e_2}(q)$ are the PESs; $v_{12,i}$ is the diabatic coupling; ω_c is the cavity frequency; $\hat{a}$ is the photon annihilation operator; and $\mathbb{P}_i = |\varphi_{0,i}\rangle\langle\varphi_{0,i}|$ is the projector onto the FC state of the i-th effective molecule. Notice that the cavity mode only couples to the transition to the $|e_1\rangle$ electronic state of the molecules. This Hamiltonian incorporates the collective interaction between the molecules and the cavity mode, neglects all single-molecule coupling effects (which is valid for ultrafast processes if single-molecule coupling strength is sufficiently weak), and neglect finite temperature effects [49].

Although the CUT-E Hamiltonian is much simpler than conventional Hamiltonians granted $N_{\text{bins}} \ll N$, it still involves the vibrational and electronic degrees of freedom of all bins. Notably, $\hat{H}'_{\text{eff}}$ can be simplified even more by mapping it to another Hamiltonian $\hat{H}_{\text{eff}}$ [Eq. (2)] whose Hilbert space

increases *linearly* with N_{bins} (see Appendix). This linear scaling is a consequence of the following considerations: first, restriction to the first excitation manifold implies that only one of the molecules is electronically excited at a time. Second, molecules in the ground electronic state do not exhibit vibrational dynamics, since the only mechanism by which they can acquire phonons is emission away from the FC region, which can be neglected in ultrafast dynamics according to CUT-E [49,50]. These two features imply that the exact wave function of the system is a superposition of states in which only one effective molecule showcases vibrational dynamics, while the other $N_{\text{bins}} - 1$ are frozen.

We assume disorder only affects the excited state PESs $V_{e,1}(q)$ and $V_{e,2}(q)$. In this way, disorder bins only appear as additional "electronic" states. This dramatic reduction of the original system into a single effective molecule showcasing $2N_{\text{bins}}$ excited electronic states is the main computational contribution of this manuscript. Its linear scaling with disorder represents a considerable improvement over methods that add an increasing number of molecules with parameters sampled from a disorder distribution, a computationally costly exercise that scales *exponentially* with N. A schematic representation of d-CUT-E is shown in Fig. 1 using two disorder bins as an example, and the mathematical procedure is explained in detail in the Appendix.

The d-CUT-E Hamiltonian reads

$$
\begin{aligned}
\hat{H}_{\text{eff}} &= \omega_c |1\rangle\langle 1| + \sum_i^{N_{\text{bins}}} \left[-\frac{1}{2}\frac{\partial^2}{\partial q^2} + V_{e_1,i}(q) \right] |e_{1,i}\rangle\langle e_{1,i}| \\
&+ \sum_i^{N_{\text{bins}}} \left[-\frac{1}{2}\frac{\partial^2}{\partial q^2} + V_{e_2,i}(q) \right] |e_{2,i}\rangle\langle e_{2,i}| \\
&+ g\sqrt{N}\sum_i^{N_{\text{bins}}} \sqrt{P_i}(|e_{1,i}\rangle\langle 1| + |1\rangle\langle e_{1,i}|)\mathbb{P} \\
&+ \sum_i^{N_{\text{bins}}} v_{12,i}|e_{1,i}\rangle\langle e_{2,i}| + \text{H.c.}.
\end{aligned}
\tag{2}
$$

Here, $\mathbb{P} = |\varphi_0\rangle\langle\varphi_0|$. The values for P_i and the parameters that define the PESs can be obtained from a disorder distribution $\rho(\omega)$.

As a proof of principle, and since we are interested in short-time processes that can be modified by strong-light matter interaction, we assume that short-time vibrational dynamics
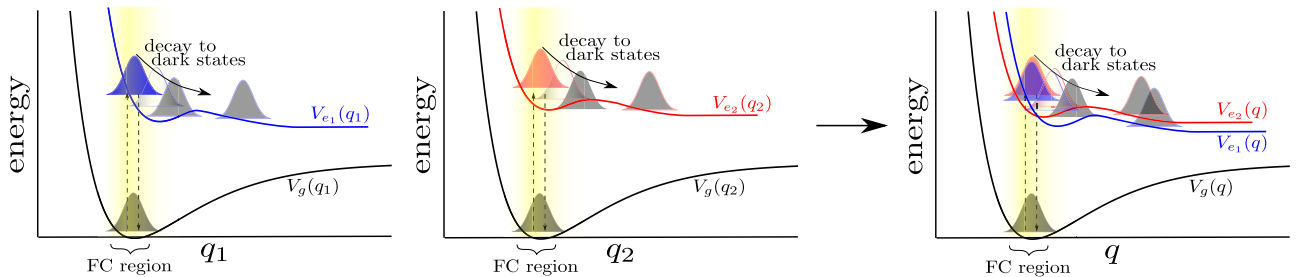

FIG. 1. Linear scaling of the dynamics with the number of disorder bins. The first two panels depict cuts of the PESs along the reaction coordinate of two different bins, q_1 and q_2. d-CUT-E projects the two-dimensional vibrational dynamics of the two bins onto a single nuclear degree of freedom q (third panel).
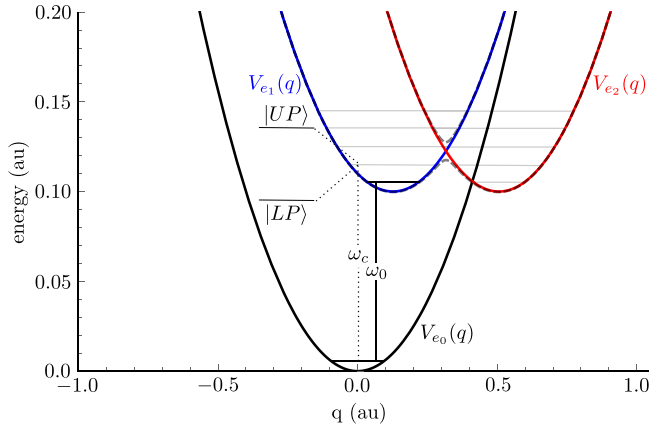
FIG. 2. Potential energy curves for the molecular system. Each molecule in our model consists of two diabatically coupled excited electronic states and one vibrational degree of freedom.

occurs only along the reaction coordinate and ignore vibrational degrees of freedom orthogonal to it [55,56]. Hence, we use a single vibrational coordinate per molecule (see Fig. 2).

The final Hamiltonian yields

$$
\hat{H}_{\text{eff}} = (\omega_c - i\kappa/2)|1\rangle\langle 1|
$$

$$
+ \sum_i^{N_{\text{bins}}} [\omega_{0,i} + \omega_{v,i}\hat{D}(s_{1,i})\hat{b}^\dagger\hat{b}\hat{D}^\dagger(s_{1,i})] \otimes |e_{1,i}\rangle\langle e_{1,i}|
$$

$$
+ \sum_i^{N_{\text{bins}}} [\omega_{0,i} + \omega_{v,i}\hat{D}(s_{2,i})\hat{b}^\dagger\hat{b}\hat{D}^\dagger(s_{2,i})] \otimes |e_{2,i}\rangle\langle e_{2,i}|
$$

$$
+ g\sqrt{N} \sum_i^{N_{\text{bins}}} \sqrt{P_i}(|e_{1,i}\rangle\langle 1| + |1\rangle\langle e_{1,i}|)\mathbb{P}
$$

$$
+ \sum_i^{N_{\text{bins}}} v_{12,i}|e_{1,i}\rangle\langle e_{2,i}| + \text{H.c.}, \tag{3}
$$

where $\hat{D}(s_{1,i}) = e^{(\hat{b}^\dagger - \hat{b})s_{1,i}}$ is the displacement operator, and $\omega_{0,i}$, $\omega_{v,i}$, and $s_{1,i}$ are the exciton frequency, vibrational frequency, and Huang-Rhys factor for the $|e_{1,i}\rangle$ electronic state, respectively. We incorporate cavity leakage by adding the imaginary term $i\kappa/2$ to the photon frequency, and the amount of energy that escapes the cavity by this mechanism can be quantified by calculating the norm of the wave function $\langle\Psi(t)|\Psi(t)\rangle$. For the rest of this work we will consider only exciton-frequency disorder. Here, disorder affects both $|e_1\rangle$ and $|e_2\rangle$ equivalently, thus the height of the barrier is the same for all bins.

To study optical effects, we calculate the linear absorption spectrum [50,57–59],

$$
A(\omega) = \kappa \, \text{Re}[\tilde{C}(\omega)] - \tfrac{1}{2}\kappa^2 |\tilde{C}(\omega)|^2, \tag{4}
$$

with $\tilde{C}(\omega) = \int_0^{T_f} dt\, e^{i\omega t}\langle\Psi(0)|\Psi(t)\rangle$ and $|\Psi(0)\rangle = |\varphi_0\rangle \otimes |1\rangle$. To study chemical effects, we calculate populations of the electronic states $|e_1\rangle$ and $|e_2\rangle$, which can be thought of as the "reactant" and "product" states of a photochemical reaction, respectively. The reaction proceeds via tunneling of the vibrational wave packet from the $|e_1\rangle$ state. We calculate
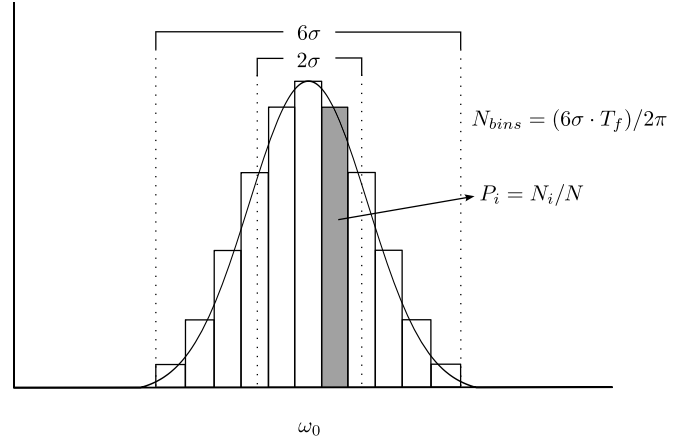

FIG. 3. Discretization of exciton frequency disorder. The frequencies follow a Gaussian distribution and the number of bins required to reach convergence is proportional to the total disorder and final propagation time.

populations for each bin, and add them up to obtain the total excited state population of reactant and product in the ensemble,

$$
P_{e_1}(t) = \sum_i^{N_{\text{bins}}} P_{e_1,i}(t) = \sum_i^{N_{\text{bins}}} \langle\Psi(t)|e_{1,i}\rangle\langle e_{1,i}|\Psi(t)\rangle,
$$

$$
P_{e_2}(t) = \sum_i^{N_{\text{bins}}} P_{e_2,i}(t) = \sum_i^{N_{\text{bins}}} \langle\Psi(t)|e_{2,i}\rangle\langle e_{2,i}|\Psi(t)\rangle. \tag{5}
$$

To capture the competition between cavity leakage and excited-state reactivity, we do not divide the expectation values by the norm.

Both optical and molecular properties are calculated for various values of exciton-frequency disorder σ and collective light-matter coupling $g\sqrt{N}$. We use the Gaussian exciton-frequency distribution $\rho(\omega) = \frac{1}{\sigma\sqrt{2\pi}}e^{-\frac{1}{2}(\frac{\omega - \omega_0}{\sigma})^2}$, with the cavity frequency being resonant with the $\nu = 0 \to \nu' = 1$ transition $\omega_c = \omega_0 + \omega_\nu$. We discretize $\rho(\omega)$ by restricting its domain to $\omega_0 - 3\sigma < \omega < \omega_0 + 3\sigma$, and calculate the values of P_i and $\omega_{0,i}$ as

$$
P_i = \int_{\omega_{i,\min}}^{\omega_{i,\max}} d\omega\,\rho(\omega) \qquad \omega_{0,i} = \int_{\omega_{i,\min}}^{\omega_{i,\max}} d\omega\,\omega\,\rho(\omega), \tag{6}
$$

with $\omega_{i,\min} = \omega_0 - 3\sigma + (i-1)(6\sigma/N_{\text{bins}})$ and $\omega_{i,\max} = \omega_0 - 3\sigma + i(6\sigma/N_{\text{bins}})$. Ignoring the tails of the distribution is justified since molecules that fall at the ends of the energy distribution are off-resonant with the cavity mode and the polariton windows (see Fig. 3).

We find that the width of the bins $\delta\omega$ required to reach convergence in optical and chemical observables obey a simple relation $\delta\omega \sim 2\pi/T_f$, where T_f is the final propagation time. This is not surprising since a finite propagation time implies a finite energy resolution. Thus, the number of bins required for convergence obeys $N_{\text{bins}} = 6\sigma(T_f/2\pi)$ (see Ref. [60] for convergence analysis). Hence, the computational cost of disorder does not scale with N, and scales linearly with $N_{\text{bins}} \propto T_f$.
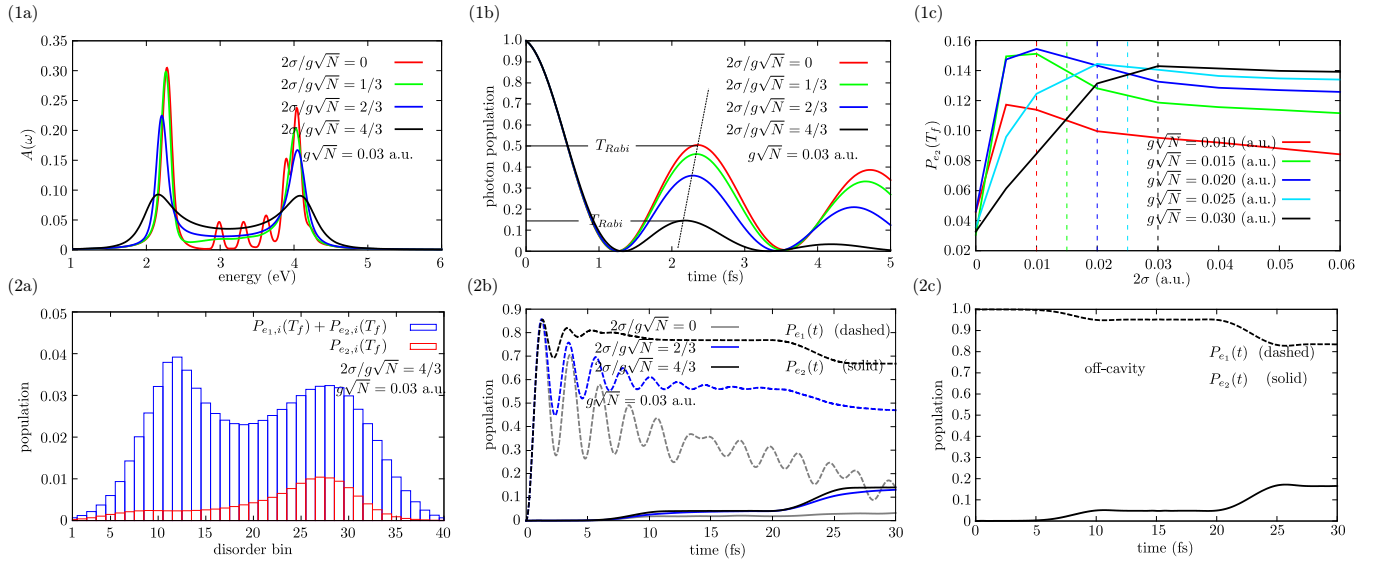
FIG. 4. Effects of exciton-frequency disorder on optical and chemical properties of molecular polaritons. Parameters: $\omega_0 = 0.10$ au, $\omega_c = 0.11$ au, $\omega_v = 0.01$ au, $\kappa = 0.006$ au, $v_{12} = 0.0025$ au, $s_1 = -1$, and $s_2 = -4$. (1a) Linear absorption spectrum for different values of disorder. Disorder suppresses vibronic features and increases the polariton Rabi splitting. (1b) Time-dependent interpretation of Rabi splitting increase caused by disorder. (1c) Final population of the electronic state $|e_2\rangle$ [$P_{e_2}(T_f)$, $T_f = 30$ fs] for different values of disorder and collective light-matter coupling strength. Vertical lines on the disorder axis correspond to $2\sigma = g\sqrt{N}$. As expected, polaritonic effects become immune to disorder for large $g\sqrt{N}$. (2a) Final excited-state populations of each disorder bin show their reaction yield (red) is different even at large disorder, and not just due to polariton modified absorption (blue). Bins are ordered from low to high exciton frequency. (2b) Population dynamics of excited electronic states $P_{e_1}(t)$ (dashed) and $P_{e_2}(t)$ (solid) for $2\sigma = 0$ (gray), $2\sigma < g\sqrt{N}$ (blue), and $2\sigma > g\sqrt{N}$ (black). (2c) Population dynamics of excited electronic states $P_{e_1}(t)$ (dashed) and $P_{e_2}(t)$ (solid) outside of the cavity. The step-like behavior in $P_{e_2}(t)$ is attributed to the reaction proceeding via tunneling of the oscillating vibrational wave packet from the $|e_1\rangle$ state. Notice the resemblance between the dynamics in (2c) and (2b) for $2\sigma/g\sqrt{N} = 2/3, 4/3$, indicating no polaritonic changes in the PESs in the presence of disorder.

III. RESULTS

Broadband excitation. Figure 4 shows optical and chemical effects of disorder for $T_f = 30$fs, $N_{\text{bins}} = 40$, and an initially photonic wave packet $|\Psi(0)\rangle = |\varphi_0\rangle \otimes |1\rangle$ (mimicking broadband excitation, $T_{\text{pulse}} \ll T_{\text{Rabi}}$). Final propagation time was chosen to avoid barrier recrossing due to the single-mode nature of our model.

Our calculations show that features that would be resolved at long timescales, such as vibronic progressions (small red peaks), vanish as disorder grows comparable to the collective light-matter coupling [Fig. 4(1a)]. This is a consequence of damping of the coherent return of population between the bright state to the cavity mode [see Fig. 4(1b)]. However, contrary to what intuition suggests, even if such dampening is significant within the timescale of the Rabi period $T_{\text{Rabi}} \sim 2.5$ fs, it does not imply that the UP and LP bands disappear. This is because only a small amplitude needs to return to the cavity (during the second half of the Rabi cycle) to create such an optical feature [61,62]. The reduction in T_{Rabi} that follows from the dampening of Rabi oscillations also leads to an increase in the Rabi splitting [37,63]. Thus, for highly disordered polaritons, collective light-matter coupling strengths *cannot* be directly extracted from polariton Rabi splitting.

Figure 4(1c) shows changes in $P_{e_2}(T_f)$ that correspond to two regimes of disorder. The low disorder regime $2\sigma < g\sqrt{N}$, characterized by a strong dependence of the reaction yield with σ, and the large disorder regime $2\sigma > g\sqrt{N}$, where the

reaction yield reaches a constant value. For low σ and low $g\sqrt{N}$ (red, green, and blue lines), disorder leads to higher total reaction yields, but this effect vanishes for large $g\sqrt{N}$ (light blue and black lines) where "polaron decoupling" takes over [11,64]. This behavior of the reaction yield in the low-disorder regime arises as a consequence of interferences between the vibrational wave packets of the electronic states for each bin $|e_{1,i}\rangle$, due to their common interaction with the photon state $|1\rangle$. These Rabi oscillations are significantly reduced at large disorder, causing the total reactivity of the ensemble to be independent of disorder. In this regime, changes of the total reaction yield upon broadband excitation for different collective coupling strengths can be explained by differences in cavity leakage (see normalized product populations [60]).

Figure 4(2a) shows that wave packet interferences in the large-disorder regime still cause differing reactivities on *individual* bins, despite them having the same PESs. By comparing the total excited state population $P_{e_1}(t) + P_{e_2}(t)$ with the product population $P_{e_2}(t)$, we conclude that this difference in product yields of individual bins cannot be attributed to differences in their respective absorption. Additional calculations show that high-frequency bins become more reactive than those at low frequency as a consequence of vibronic coupling of the $|e_1\rangle$ electronic state (here, $s_1 = -1$), and that this effect is suppressed if $s_1 = 0$ (see Ref. [60]). We will elaborate on the consequences of this effect when we consider narrowband excitation. Figure 4(2b) shows time-dependent total population dynamics for zero, intermediate,
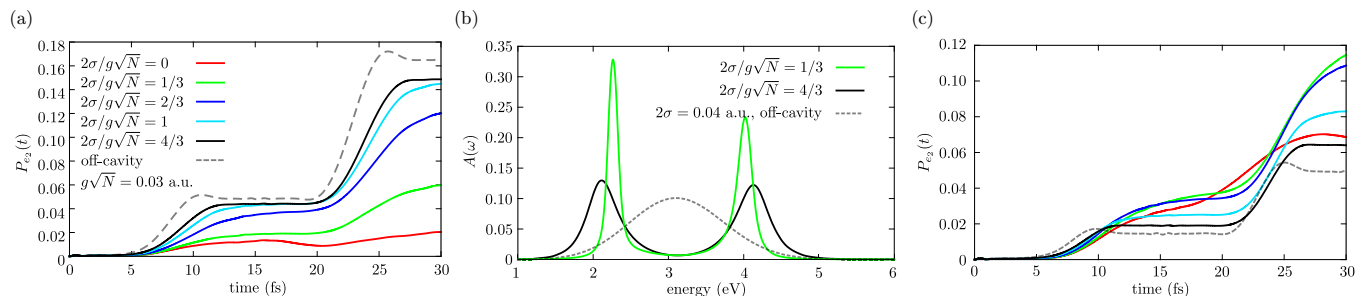
FIG. 5. Reaction yield in the strong-coupling regime as a function of disorder upon broadband excitation (bright initial state). (a) Reaction is suppressed with strong coupling; however, as disorder becomes comparable to the Rabi splitting, $P_{e_2}(t)$ resembles the behavior outside of the cavity. (b) Absorption spectrum $A(\omega)$ for the dynamics in (a): strong coupling low disorder (green), strong coupling large disorder (black), and outside of the cavity (dashed). Notably, despite well-defined polariton bands for large disorder, the corresponding reactivity in (a) is similar to the off-cavity case. (c) Same as (a) but shifting the PES of $|e_2\rangle$ upward by two vibrational quanta. In this case, strong coupling enhances the reaction for weak disorder.

and large disorder. In the absence of disorder, strong light-matter coupling gives rise to large amplitude Rabi oscillations for $P_{e_1}(t)$ that last even after the reaction occurs, producing a low reaction yield. This polaritonic-induced reduction of reactivity (polaron decoupling) has been explained in previous theoretical works as a change in the PESs that prevents the nuclei from moving away from the FC [11,53,64,65]. However, for intermediate and large disorder, Rabi oscillations are damped before the reaction ensues, polaron decoupling disappears, and the reactivity reaches a constant value. This constant value corresponds to the reaction yield outside of the cavity, as shown in Fig. 4(2c), where we have initiated the system in the bright state $|\Psi(0)\rangle = \sum_i^{N_{bins}} \sqrt{P_i}|\varphi_0\rangle \otimes |e_i\rangle$, for $g\sqrt{N} = 0$. From this we conclude that changes in the reaction yield upon broadband excitation are not possible if reactivity occurs on a timescale longer than that of Rabi oscillations, even if the linear absorption spectrum showcases two clear polariton bands [see Fig. 4(a)].

Next, we systematically study how the large-disorder regime approaches the off-cavity limit by initiating the dynamics in the bright state and calculating the total excited states populations for $g\sqrt{N} = 0.03$ au, increasing the disorder. This allows us to directly compare the ensuing dynamics with that outside of the cavity ($g\sqrt{N} = 0$). Importantly, the out-of-cavity population dynamics is independent of disorder for these initial conditions.

We find that broadband excitation in the large-disorder regime does not result in different photochemistry than outside of the cavity, although the linear absorption spectrum misleadingly suggests otherwise. As we discussed before, this occurs because, even for large disorder, the Rabi splitting in the absorption spectrum is a feature defined at short times ($T \sim 2.5$ fs), for which disorder has a very minor effect. On the contrary, at the longer timescales of chemical reactivity, disorder has already caused decoherence of wave function in individual disorder bins. We also modified the PES of $|e_2\rangle$ so that it lies at higher energies with respect to $|e_1\rangle$. Contrary to the previous scenario, for low disorder, we observe a polariton-mediated increase in the total reaction yield if the target state $|e_2\rangle$ is 0.02 au blue detuned with respect to $|e_1\rangle$, thanks to the UP having high enough energy to allow the barrier crossing. Moreover, we observe that the behavior is not monotonic and population transfer is enhanced for low values of disorder, but eventually converges to the dynamics outside of the cavity [see Fig. 5(c)].

Narrowband excitation. We next examine selective excitation of either one of the polariton bands (narrowband excitation, $T_{pulse} > T_{Rabi}$). To this end, we initiate the dynamics in the states $|\Psi_\pm(0)\rangle = \frac{1}{\sqrt{2}}|\varphi_0\rangle \otimes (|1\rangle \pm \sum_i^{N_{bins}} \sqrt{P_i}|e_i\rangle)$, which allocate the same vibrational energy to all bins, and their average energy is that of the polaritons.
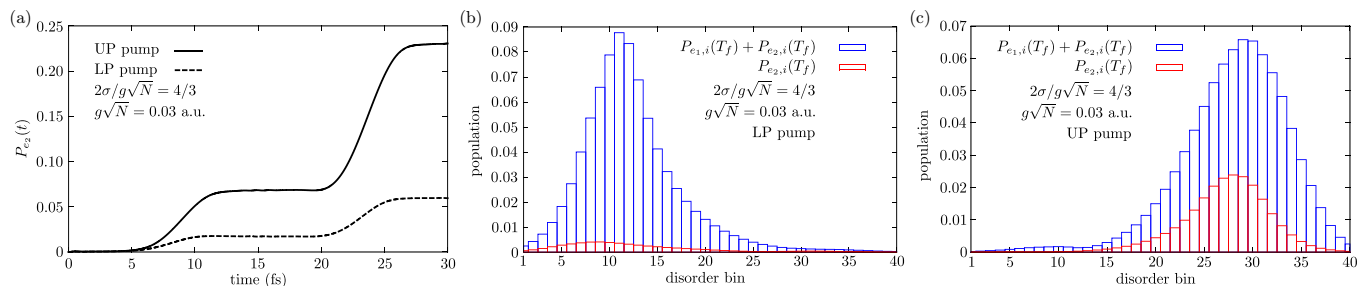

FIG. 6. Reaction yield upon narrowband excitation in the strong-coupling and large-disorder regime (parameters: $g\sqrt{N} = 0.03$ au and $2\sigma = 0.04$ au). (a) Total product state population after pumping the UP (solid) and the LP (dashed). (b) and (c) Excited-state populations of each disorder bin showing their reaction yield (red) and absorption (blue), after LP pumping and UP pumping. Larger ratios $P_{e_2,i}(T_f)/[P_{e_1,i}(T_f) + P_{e_2,i}(T_f)]$ imply higher reactivity. (b) and (c) indicate that the higher reactivity of the UP bins cannot be explained simply by polariton absorption, which slightly favors the LP bins.
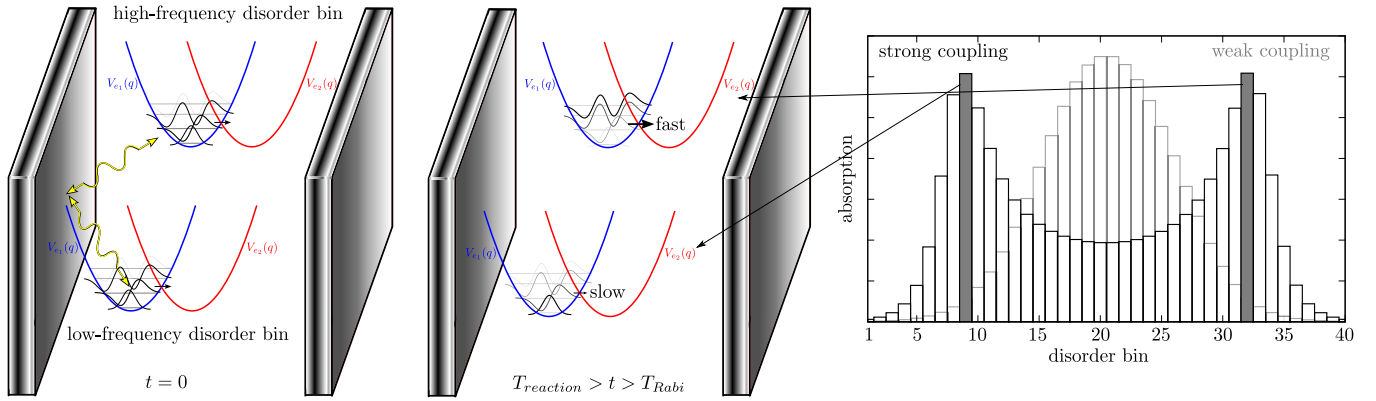
FIG. 7. Mechanism of frequency-dependent photoreactivity in disordered molecular polaritons. Interplay of narrowband excitation and cavity-mediated interactions between disorder bins results in the preparation of states with different reactivities after damping of Rabi oscillations and before the chemical reaction. These highly (slightly) reactive bins can be excited at the UP (LP) frequency, leading to an increase (decrease) of the total reactivity upon narrowband excitation.

Figure 6 shows that selective pumping of polariton bands yields different excited-state reaction yields. As we might expect from Fig. 4(2a), excitation of the UP results in a high reaction yield due to selective excitation of the bins with a higher reactivity, while excitation of the LP results in a low reaction yield. This can be explained as a cavity-assisted mixing of high-lying vibronic states of the low-energy bins with low-lying vibronic states of the high-frequency bins through Rabi oscillations, resulting in excitation of molecules near the UP with more vibrational energy, and molecules near the LP with lower vibrational energy. A scheme of this mechanism is shown in Fig. 7, and numerical evidence is provided in the Supplemental Material [60]. Notice that this mechanism is a consequence of the definition of the initial excited state. Since the laser pulse must be longer than the Rabi period to selectively excite a single polariton band, both the external laser and polariton dynamics simultaneously participate in the creation of the initial states with differing reactivities. Crucially, there is no reason to believe that these highly reactive states cannot be created without the cavity's presence using a *different* narrowband linear external laser that efficiently targets high-energy vibronic progressions through the UP (LP) band. In fact, both strategies rely on nonzero vibronic coupling to produce frequency-dependent photoreactivity. Therefore, whether collective strong coupling in the large N limit provides any advantage to control chemical reactivity compared to conventional linear optical sources is not readily apparent, especially in light of recent experiments that suggest there are no polaritonic effects on chemical dynamics [66,67].

IV. SUMMARY

We have successfully introduced the d-CUT-E method to efficiently simulate the ultrafast dynamics of disordered molecular ensembles under collective strong coupling. Our findings challenge the notion that a Rabi splitting in the linear absorption spectrum inevitably implies changes in chemical reactivity. This is due to the disparity in timescales governing optical and chemical properties. Optical properties primarily manifest at short timescales when disorder has minimal impact, while chemical properties emerge at longer timescales. In the common scenario that disorder is comparable with the light-matter coupling strength, strong coupling induces modifications in the reactivity of individual disorder bins, which can be selectively targeted by narrowband pulses. This phenomenon should be interpreted as a cavity-mediated initial state preparation effect.

APPENDIX: CUT-E HAMILTONIAN IN THE LARGE N LIMIT FOR DISCRETE DISORDER

For simplicity, let us derive $\hat{H}_{\text{eff}}$ when there is a single electronic excited state per molecule. The general polariton Hamiltonian yields

$$\hat{H} = \sum_i^N \left(\hat{H}_{\text{mol}}^{(i)} + \hat{H}_I^{(i)} \right) + \hat{H}_{\text{cav}}, \tag{A1}$$

where the Hamiltonians $\hat{H}_{\text{mol}}^{(i)}$, $\hat{H}_{\text{cav}}$, and $\hat{H}_I^{(i)}$ describe the energy of the i-th molecule, the cavity mode, and the light-matter interaction. In our work we use a simple model that assumes a single-cavity mode and neglects intermolecular interactions, leading to

$$\begin{aligned}
\hat{H}_{\text{mol}}^{(i)} &= \hat{h}_g^{(i)} |g_i\rangle\langle g_i| + \hat{h}_e^{(i)} |e_i\rangle\langle e_i|, \\
&= -\frac{1}{2}\frac{\partial^2}{\partial q_i^2}\mathbb{1} + V_{g,i}(q_i)|g_i\rangle\langle g_i| + V_{e,i}(q_i)|e_i\rangle\langle e_i|, \\
\hat{H}_{\text{cav}} &= \omega_c \hat{a}^\dagger \hat{a}, \\
\hat{H}_I^{(i)} &= g(|e_i\rangle\langle g_i|\hat{a} + |g_i\rangle\langle e_i|\hat{a}^\dagger).
\end{aligned} \tag{A2}$$

In a previous work, we showed that, assuming all molecules are in their global ground state and taking the

large N limit (zeroth-order approximation in CUT-E, single-molecule light matter coupling $g \to 0$ while keeping $g\sqrt{N}$ constant), the time-dependent wave function in the first excitation manifold can be obtained by solving a simple system of equations of motion (EoM) [49]:

$$i\dot{A}^{(0)}_{00\ldots0}(t) = \omega_c A^{(0)}_{00\ldots0}(t) + g\sum_{i=1}^{N}\sum_{l_i}\langle\varphi_0|\phi_{l_i}\rangle A^{(i)}_{00\ldots l_i\ldots0}(t)$$

$$i\dot{A}^{(i)}_{00\ldots l_i\ldots0}(t) = \left(\omega_{0,i} + \omega^{(i)}_{v,l_i}\right)A^{(i)}_{00\ldots l_i\ldots0}(t)$$
$$+ g\sum_{l_i}\langle\phi_{l_i}|\varphi_0\rangle A^{(0)}_{00\ldots0}(t), \tag{A3}$$

where $A^{(0)}_{00\ldots0}$ is the amplitude of the state with all molecules in the global ground state and 1 photon in the cavity (superscript 0 indicates cavity) $|1\rangle|\varphi_{0,1}\rangle|\varphi_{0,2}\rangle\cdots|\varphi_{0,N}\rangle$ with frequency ω_c, while $A^{(i)}_{00\ldots l_i\ldots0}(t)$ is the amplitude of the state where molecule i is excited in the vibrational state l_i, $|e_i\rangle|\varphi_{0,1}\rangle|\varphi_{0,2}\rangle\cdots|\phi_{l_i,i}\rangle\cdots|\varphi_{0,N}\rangle$, with frequency $\omega_{0,i} + \omega^{(i)}_{v,l_i}$. Contribution of other states to the total wave function vanish at large N [19,49,50].

If the total molecular ensemble consists of N_{bins} groups composed of N_i identical molecules each, we can rewrite the EoM as

$$i\dot{A}^{(0)}_{00\ldots0}(t) = \omega_c A^{(0)}_{00\ldots0}(t) + g\sum_{i=1}^{N_{\text{bins}}}N_i\sum_{l_i}\langle\varphi_{0,i}|\phi_{l_i,i}\rangle A^{(i)}_{00\ldots l_i\ldots0}(t)$$

$$i\dot{A}^{(i)}_{00\ldots l_i\ldots0}(t) = \left(\omega_{0,i} + \omega^{(i)}_{v,l_i}\right)A^{(i)}_{00\ldots l_i\ldots0}(t)$$
$$+ g\sum_{l_i}\langle\phi_{l_i,i}|\varphi_{0,i}\rangle A^{(0)}_{00\ldots0}(t), \tag{A4}$$

where i now runs over the disorder bins and $\sum_i N_i = N$.

By renormalizing the exciton coefficients as $\tilde{A}^{(i)}_{00\ldots l_i\ldots0}(t) = \sqrt{N_i}A^{(i)}_{00\ldots l_i\ldots0}(t)$, we get

$$i\dot{A}^{(0)}_{00\ldots0}(t) = \omega_c A^{(0)}_{00\ldots0}(t) + g\sqrt{N}\sum_{i=1}^{N_{\text{bins}}}\sqrt{P_i}$$
$$\times \sum_{l_i}\langle\varphi_{0,i}|\phi_{l_i,i}\rangle\tilde{A}^{(i)}_{00\ldots l_i\ldots0}(t)$$

$$i\dot{\tilde{A}}^{(i)}_{00\ldots l_i\ldots0}(t) = \left(\omega_{0,i} + \omega^{(i)}_{v,l_i}\right)\tilde{A}^{(i)}_{00\ldots l_i\ldots0}(t) + g\sqrt{N}\sqrt{P_i}$$
$$\times \sum_{l_i}\langle\phi_{l_i,i}|\varphi_{0,i}\rangle A^{(0)}_{00\ldots0}(t), \tag{A5}$$

with $P_i = N_i/N$. These EoM yield the effective Hamiltonian

$$\hat{H}'_{\text{eff}} = \omega_c|1\rangle\langle1| + \sum_{i}^{N_{\text{bins}}}\hat{H}_{e,i}(q_i)|e_i\rangle\langle e_i|$$
$$+ g\sqrt{N}\sum_{i}^{N_{\text{bins}}}\sqrt{P_i}(|e_i\rangle\langle1| + |1\rangle\langle e_i|)\mathbb{P}_i. \tag{A6}$$

The vibrational projector $\mathbb{P}_i = |\varphi_{0,i}\rangle\langle\varphi_{0,i}|$ implies that the strong light-matter interaction only occurs at the Franck-Condon region. Notice that $\hat{H}'_{\text{eff}}$ spans the Hilbert space formed by the vibrational and electronic degrees of freedom of all molecules. Equation (1) in the manuscript is just an extension of this Hamiltonian, acknowledging the product state $|e_2\rangle$ and the diabatic coupling between reactant and product v_{12} (see Fig. 2).

In this article, we are only interested in local observables (e.g., excited state populations); hence, we can directly compute them from the effective wave function evolving according to $\hat{H}'_{\text{eff}}$ [see Ref. [49], Eq. (23)]. However, $\hat{H}'_{\text{eff}}$ can be further simplified. This becomes clearer if we assume the Franck-Condon state is identical for each effective molecule, i.e., $|\varphi_{0,i}\rangle \to |\varphi_0\rangle$,

$$i\dot{A}^{(0)}_{00\ldots0}(t) = \omega_c A^{(0)}_{00\ldots0}(t) + g\sqrt{N}\sum_{i=1}^{N_{\text{bins}}}\sqrt{P_i}$$
$$\times \sum_{l_i}\langle\varphi_0|\phi_{l_i,i}\rangle\tilde{A}^{(i)}_{00\ldots l_i\ldots0}(t)$$

$$i\dot{\tilde{A}}^{(i)}_{00\ldots l_i\ldots0}(t) = \left(\omega_{0,i} + \omega^{(i)}_{v,l_i}\right)\tilde{A}^{(i)}_{00\ldots l_i\ldots0}(t) + g\sqrt{N}\sqrt{P_i}$$
$$\times \sum_{l_i}\langle\phi_{l_i,i}|\varphi_0\rangle A^{(0)}_{00\ldots0}(t). \tag{A7}$$

One can check that the following effective Hamiltonian and wave function leads to the EoM above,

$$\hat{H}_{\text{eff}} = \omega_c|1\rangle\langle1| + \sum_{i}^{N_{\text{bins}}}\hat{H}_{e,i}(q)|e_i\rangle\langle e_i| + g\sqrt{N}$$
$$\times \sum_{i}^{N_{\text{bins}}}\sqrt{P_i}(|e_i\rangle\langle1| + |1\rangle\langle e_i|)\mathbb{P},$$

$$|\tilde{\Psi}(t)\rangle = A^{(0)}_{00\ldots0}(t)|\varphi_0\rangle \otimes |1\rangle$$
$$+ \sum_{i}\sum_{l_i}\tilde{A}^{(i)}_{00\ldots l_i\ldots0}(t)|\phi_{l_i,i}\rangle \otimes |e_i\rangle. \tag{A8}$$

This effective Hamiltonian spans the Hilbert space formed by N_{bins} electronic states, but only the vibrational degrees of freedom of a single molecule (see Fig. 1). Again, we can directly compute local observables from the effective wave function evolving according to $\hat{H}_{\text{eff}}$. Alternatively, it can be interpreted as pertaining to a single effective molecule with N_{bins} electronic states. This reduction in the electronic and vibrational degrees of freedom is a dramatic simplification compared to the original Hamiltonian in Eq. (A1).

The Hamiltonian in Eq. (3) of the manuscript is an extension of $\hat{H}_{\text{eff}}$ for two electronic excited states diabatically coupled and one vibrational mode per molecule.

[1] J. A. Hutchison, T. Schwartz, C. Genet, E. Devaux, and T. W. Ebbesen, Modifying chemical landscapes by coupling to vacuum fields, Angew. Chem. Int. Ed. **51**, 1592 (2012).

[2] H. Zeng, J. B. Pérez-Sánchez, C. T. Eckdahl, P. Liu, W. J. Chang, E. A. Weiss, J. A. Kalow, J. Yuen-Zhou, and N. P. Stern, Control of photoswitching kinetics with strong

lightmatter coupling in a cavity, J. Am. Chem. Soc. **145**, 19655 (2023).

[3] W. Ahn, J. F. Triana, F. Recabal, F. Herrera, and B. S. Simpkins, Modification of ground-state chemical reactivity via light-matter coherence in infrared cavities, Science **380**, 1165 (2023).

[4] A. D. Dunkelberger, B. S. Simpkins, I. Vurgaftman, and J. C. Owrutsky, Vibration-cavity polariton chemistry and dynamics, Annu. Rev. Phys. Chem. **73**, 429 (2022).

[5] R. F. Ribeiro, L. A. Martínez-Martínez, M. Du, J. Campos-Gonzalez-Angulo, and J. Yuen-Zhou, Polariton chemistry: controlling molecular dynamics with optical cavities, Chem. Sci. **9**, 6325 (2018).

[6] B. Xiang, R. F. Ribeiro, M. Du, L. Chen, Z. Yang, J. Wang, J. Yuen-Zhou, and W. Xiong, Intermolecular vibrational energy transfer enabled by microcavity strong light-matter coupling, Science **368**, 665 (2020).

[7] T.-T. Chen, M. Du, Z. Yang, J. Yuen-Zhou, and W. Xiong, Cavity-enabled enhancement of ultrafast intramolecular vibrational redistribution over pseudorotation, Science **378**, 790 (2022).

[8] J. A. Campos-Gonzalez-Angulo, Y. R. Poh, M. Du, and J. Yuen-Zhou, Swinging between shine and shadow: Theoretical advances on thermally activated vibropolaritonic chemistry, J. Chem. Phys. **158**, 230901 (2023).

[9] A. Mandal and P. Huo, Investigating new reactivities enabled by polariton photochemistry, J. Phys. Chem. Lett. **10**, 5519 (2019).

[10] F. Herrera and J. Owrutsky, Molecular polaritons for controlling chemistry with quantum optics, J. Chem. Phys. **152**, 100902 (2020).

[11] J. Galego, F. J. Garcia-Vidal, and J. Feist, Suppressing photochemical reactions with quantized light fields, Nat. Commun. **7**, 13841 (2016).

[12] M. Sánchez-Barquilla, A. I. Fernández-Domínguez, J. Feist, and F. J. García-Vidal, A theoretical perspective on molecular polaritonics, ACS Photon. **9**, 1830 (2022).

[13] M. Reitz, C. Sommer, and C. Genes, Langevin approach to quantum optics with molecules, Phys. Rev. Lett. **122**, 203602 (2019).

[14] A. Mandal, M. Taylor, B. Weight, E. Koessler, X. Li, and P. Huo, Theoretical advances in polariton chemistry and molecular cavity quantum electrodynamics, ChemRxiv (2022).

[15] T. Ishii, F. Bencheikh, S. Forget, S. Chénais, B. Heinrich, D. Kreher, L. Sosa Vargas, K. Miyata, K. Onda, T. Fujihara, S. Kéna-Cohen, F. Mathevet, and C. Adachi, Enhanced light-matter interaction and polariton relaxation by the control of molecular orientation, Adv. Opt. Mater. **9**, 2101048 (2021).

[16] C. R. Gubbin, S. A. Maier, and S. Kéna-Cohen, Low-voltage polariton electroluminescence from an ultrastrongly coupled organic light-emitting diode, Appl. Phys. Lett. **104**, 233302 (2014).

[17] T. E. Li and S. Hammes-Schiffer, QM/MM modeling of vibrational polariton induced energy transfer and chemical dynamics, J. Am. Chem. Soc. **145**, 377 (2023).

[18] F. C. Spano, Optical microcavities enhance the exciton coherence length and eliminate vibronic coupling in J-aggregates, J. Chem. Phys. **142**, 184707 (2015).

[19] F. C. Spano, Exciton-phonon polaritons in organic microcavities: Testing a simple ansatz for treating a large number of chromophores, J. Chem. Phys. **152**, 204113 (2020).

[20] Z. Zhang and S. Mukamel, Fluorescence spectroscopy of vibronic polaritons of molecular aggregates in optical microcavities, Chem. Phys. Lett. **683**, 653 (2017).

[21] R. F. Ribeiro, Multimode polariton effects on molecular energy transport and spectral fluctuations, Commun. Chem. **5**, 48 (2022).

[22] A. Mandal, D. Xu, A. Mahajan, J. Lee, M. Delor, and D. R. Reichman, Microscopic theory of multimode polariton dispersion in multilayered materials, Nano Lett. **23**, 4082 (2023).

[23] G. Engelhardt and J. Cao, Unusual dynamical properties of disordered polaritons in microcavities, Phys. Rev. B **105**, 064205 (2022).

[24] O. Vendrell and H.-D. Meyer, Multilayer multiconfiguration time-dependent Hartree method: Implementation and applications to a Henon-Heiles Hamiltonian and to pyrazine, J. Chem. Phys. **134**, 044135 (2011).

[25] L. Lacombe, N. M. Hoffmann, and N. T. Maitra, Exact potential energy surface for molecules in cavities, Phys. Rev. Lett. **123**, 083201 (2019).

[26] R. H. Tichauer, J. Feist, and G. Groenhof, Multi-scale dynamics simulations of molecular polaritons: The effect of multiple cavity modes on polariton relaxation, J. Chem. Phys. **154**, 104112 (2021).

[27] H. L. Luk, J. Feist, J. J. Toppari, and G. Groenhof, Multi-scale molecular dynamics simulations of polaritonic chemistry, J. Chem. Theory Comput. **13**, 4324 (2017).

[28] M. A. Sentef, M. Ruggenthaler, and A. Rubio, Cavity quantum-electrodynamical polaritonically enhanced electron-phonon coupling and its influence on superconductivity, Sci. Adv. **4**, eaau6969 (2018).

[29] C. Schäfer, M. Ruggenthaler, H. Appel, and A. Rubio, Modification of excitation and charge transfer in cavity quantum-electrodynamical chemistry, Proc. Natl. Acad. Sci. USA **116**, 4883 (2019).

[30] D. Sidler, C. Schäfer, M. Ruggenthaler, and A. Rubio, Polaritonic chemistry: Collective strong coupling implies strong local modification of chemical properties, J. Phys. Chem. Lett. **12**, 508 (2021).

[31] M. Sukharev, J. Subotnik, and A. Nitzan, Dissociation slow-down by collective optical response under strong coupling conditions, J. Chem. Phys. **158**, 084104 (2023).

[32] S. Mondal, D. S. Wang, and S. Keshavamurthy, Dissociation dynamics of a diatomic molecule in an optical cavity, J. Chem. Phys. **157**, 244109 (2022).

[33] R. Houdré, R. P. Stanley, and M. Ilegems, Vacuum-field Rabi splitting in the presence of inhomogeneous broadening: Resolution of a homogeneous linewidth in an inhomogeneously broadened system, Phys. Rev. A **53**, 2711 (1996).

[34] D. Wellnitz, G. Pupillo, and J. Schachenmayer, Disorder enhanced vibrational entanglement and dynamics in polaritonic chemistry, Commun. Phys. **5**, 120 (2022).

[35] M. F. Gelin, A. Velardo, and R. Borrelli, Efficient quantum dynamics simulations of complex molecular systems: A unified treatment of dynamic and static disorder, J. Chem. Phys. **155**, 134102 (2021).

[36] K. Sun, C. Dou, M. F. Gelin, and Y. Zhao, Dynamics of disordered Tavis-Cummings and Holstein-Tavis-Cummings models, J. Chem. Phys. **156**, 024102 (2022).

[37] B. Cohn, S. Sufrin, A. Basu, and L. Chuntonov, Vibrational polaritons in disordered molecular ensembles, J. Phys. Chem. Lett. **13**, 8369 (2022).

[38] A. G. Avramenko and A. S. Rury, Light emission from vibronic polaritons in coupled metalloporphyrin-multimode cavity systems, J. Phys. Chem. Lett. **13**, 4036 (2022).

[39] M. Tokman, A. Behne, B. Torres, M. Erukhimova, Y. Wang, and A. Belyanin, Dissipation-driven formation of entangled dark states in strongly coupled inhomogeneous many-qubit systems in solid-state nanocavities, Phys. Rev. A **107**, 013721 (2023).

[40] G. Engelhardt and J. Cao, Polariton localization and dispersion properties of disordered quantum emitters in multimode microcavities, Phys. Rev. Lett. **130**, 213602 (2023).

[41] A. M. Alvertis, R. Pandya, C. Quarti, L. Legrand, T. Barisien, B. Monserrat, A. J. Musser, A. Rao, A. W. Chin, and D. Beljonne, First principles modeling of exciton-polaritons in polydiacetylene chains, J. Chem. Phys. **153**, 084103 (2020).

[42] F. Fassioli, K. H. Park, S. E. Bard, and G. D. Scholes, Femtosecond photophysics of molecular polaritons, J. Phys. Chem. Lett. **12**, 11444 (2021).

[43] D. Xu, A. Mandal, J. M. Baxter, S.-W. Cheng, I. Lee, H. Su, S. Liu, D. R. Reichman, and M. Delor, Ultrafast imaging of polariton propagation and interactions, Nat. Commun. **14**, 3881 (2023).

[44] E. Suyabatmaz and R. F. Ribeiro, Vibrational polariton transport in disordered media, J. Chem. Phys. **159**, 034701 (2023).

[45] T. F. Allard and G. Weick, Disorder-enhanced transport in a chain of lossy dipoles strongly coupled to cavity photons, Phys. Rev. B **106**, 245424 (2022).

[46] R. Pandya, A. Ashoka, K. Georgiou, J. Sung, R. Jayaprakash, S. Renken, L. Gai, Z. Shen, A. Rao, and A. J. Musser, Tuning the coherent propagation of organic exciton-polaritons through dark state delocalization, Adv. Sci. **9**, 2105569 (2022).

[47] H.-T. Chen, Z. Zhou, M. Sukharev, J. E. Subotnik, and A. Nitzan, Interplay between disorder and collective coherent response: Superradiance and spectral motional narrowing in the time domain, Phys. Rev. A **106**, 053703 (2022).

[48] N. Krainova, A. J. Grede, D. Tsokkou, N. Banerji, and N. C. Giebink, Polaron photoconductivity in the weak and strong light-matter coupling regime, Phys. Rev. Lett. **124**, 177401 (2020).

[49] J. B. Pérez-Sánchez, A. Koner, N. P. Stern, and J. Yuen-Zhou, Simulating molecular polaritons in the collective regime using few-molecule models, Proc. Natl. Acad. Sci. USA **120**, e2219223120 (2023).

[50] M. A. Zeb, P. G. Kirton, and J. Keeling, Exact states and spectra of vibrationally dressed polaritons, ACS Photon. **5**, 249 (2018).

[51] M. A. Zeb, Efficient linear scaling mapping for permutation symmetric Fock spaces, Comput. Phys. Commun. **276**, 108347 (2022).

[52] M. A. Zeb, P. G. Kirton, and J. Keeling, Incoherent charge transport in an organic polariton condensate, Phys. Rev. B **106**, 195109 (2022).

[53] B. Cui and A. Nizan, Collective response in light-matter interactions: The interplay between strong coupling and local dynamics, J. Chem. Phys. **157**, 114108 (2022).

[54] B. Gu, Toward collective chemistry by strong light-matter coupling, arXiv:2306.08944.

[55] N. Anto-Sztrikacs and D. Segal, Capturing non-Markovian dynamics with the reaction coordinate method, Phys. Rev. A **104**, 052617 (2021).

[56] L. S. Cederbaum, E. Gindensperger, and I. Burghardt, Short-time dynamics through conical intersections in macrosystems, Phys. Rev. Lett. **94**, 113003 (2005).

[57] J. A. Cwik, P. Kirton, S. De Liberato, and J. Keeling, Excitonic spectral features in strongly coupled organic polaritons, Phys. Rev. A **93**, 033840 (2016).

[58] F. Herrera and F. C. Spano, Absorption and photoluminescence in organic cavity QED, Phys. Rev. A **95**, 053867 (2017).

[59] J. Yuen-Zhou and A. Koner, Linear response of molecular polaritons, arXiv:2310.15424.

[60] See Supplemental Material at http://link.aps.org/supplemental/10.1103/PhysRevResearch.6.013222 for convergence analysis, effects of cavity leakage in the total reactivity, normalized product population, reactivity of disorder bins as a function of collective coupling strength, barrier height, and vibronic coupling.

[61] E. J. Heller, The semiclassical way to molecular spectroscopy, Acc. Chem. Res. **14**, 368 (1981).

[62] D. Tannor, *Introduction to Quantum Mechanics: A Time Dependent Perspective* (University Science Books, Melville, 2007).

[63] T. Gera and K. L. Sebastian, Effects of disorder on polaritonic and dark states in a cavity using the disordered Tavis-Cummings model, J. Chem. Phys. **156**, 194304 (2022).

[64] F. Herrera and F. C. Spano, Cavity-controlled chemistry in molecular ensembles, Phys. Rev. Lett. **116**, 238301 (2016).

[65] J. Kuttruff, M. Romanelli, E. Pedrueza-Villalmanzo, J. Allerbeck, J. Fregoni, V. Saavedra-Becerril, J. Andréasson, D. Brida, A. Dmitriev, S. Corni, and N. Maccaferri, Sub-picosecond collapse of molecular polaritons to pure molecular transition in plasmonic photoswitch-nanoantennas, Nat. Commun. **14**, 3875 (2023).

[66] P. A. Thomas, W. J. Tan, V. G. Kravets, A. N. Grigorenko, and W. L. Barnes, Non-polaritonic effects in cavity-modified photochemistry, Adv. Mater. **36**, 2309393 (2024).

[67] A. Dutta, V. Tiainen, L. Duarte, N. Markesevic, D. Morozov, H. A. Qureshi, G. Groenhof, and J. J. Toppari, Ultra-fast photochemistry in the strong light-matter coupling regime, ChemRxiv. (2023).

Correction: The previously published order of authors was presented incorrectly and has been fixed.